JOURNAL OF SPACECRAFT AND ROCKETS
Vol. 37, No. 5, September–October 2000

Engineering Notes

ENGINEERING NOTES are short manuscripts describing new developments or important results of a preliminary nature. These Notes cannot exceed six manuscript pages and three figures; a page of text may be substituted for a figure and vice versa. After informal review by the editors, they may be published within a few months of the date of receipt. Style requirements are the same as for regular contributions (see inside back cover).

Comet Rendezvous Mission Design Using Solar Electric Propulsion Spacecraft

C. A. Kluever*
University of Missouri–Columbia, Columbia, Missouri 65211

Introduction

SOLAR electric propulsion (SEP) has become a viable propulsion option for performing interplanetary space missions after its successful demonstration by the first new millennium mission, Deep Space 1 (DS1).[1] Several investigators have recently studied the use of SEP for interplanetary missions to Mars,[2] Mercury,[3,4] Jupiter,[4] main-belt asteroids,[4] and short-period comets.[4,5] This Note investigates the feasibility of using SEP for a rendezvous trajectory with the comet Wilson-Harrington (WH). In Ref. 5 Sims presents both optimal rendezvous and sample return trajectories to the comets Brooks 2 and Wirtanen. The mission analysis in this Note incorporates a detailed treatment of the spacecraft system mass breakdown in the trajectory optimization process. Furthermore, the mission design presented here includes additional constraints on the comet rendezvous date for enhanced scientific payoff, as well as lifetime considerations for the ion thrusters. For this analysis two-body dynamics govern the orbit transfer, and an Earth gravity assist increases the orbital energy and conserves propellant. Numerical results are presented for maximum payload trajectories.

Trajectory Optimization

The comet mission design objective is to maximize the spacecraft's payload mass at rendezvous with the target comet Wilson-Harrington. The interplanetary trajectory begins with injection into heliocentric space by a Delta launch vehicle. A fixed structure for the number and sequence of engine burns/coasts and planetary flybys is assumed. The design variables include launch date, injection point in low-Earth orbit, launch energy C_3, input power to the ion thrusters at 1 astronomical unit (AU) from the sun P_0, SEP thrust arc durations, thrust direction during the powered arcs, coast arc angles, planetary flyby conditions, and rendezvous date. Whereas a patched-conic approach is used to model the orbit transfer, the powered equations of motion are numerically integrated by using a fixed-step, fourth-order Runge–Kutta routine. Coast arcs are computed analytically. The planetary gravity assist is modeled as a ΔV impulse (without change in spacecraft heliocentric position) and is defined by selecting the periapsis radius and orbit plane orientation for the flyby. Details of the numerical simulation of the interplanetary trajectory are presented in Ref. 6.

Numerical solutions of the maximum-payload problem are obtained by using a direct trajectory optimization method.[6] The optimal control problem is replaced by a nonlinear programming problem, which is solved by using sequential quadratic programming (SQP), a constrained parameter optimization method. The SQP code used here is taken from Ref. 7 and uses forward finite differences to compute gradient information. The thrust direction is defined by three direction cosines relative to a rotating radial-transverse-normal frame, and the time histories of these direction cosines are parameterized by linear interpolation through a set of discrete nodes. The rendezvous conditions are imposed by six SQP equality constraints that maintain a match between the orbital elements of the spacecraft and WH at the final time. Three additional SQP equality constraints maintain a position match between the spacecraft and Earth at the gravity assist. The orbital elements of the Earth and WH are computed using a solar system ephemeris from the low-thrust program VARITOP.[8] Finally, an SQP inequality constraint for the total allowable xenon propellant mass is included in the optimization problem to account for the expected lifetime of an ion thruster. The ion engine for the DS1 spacecraft can safely eject 80 kg of propellant before grid erosion degrades thruster reliability. Therefore, the maximum xenon propellant is limited to 80, 160, and 240 kg for spacecraft configurations with one, two, and three thrusters, respectively.

Spacecraft System Analysis

A detailed account of the mass contribution from each spacecraft system is presented in Table 1. All system masses are either scaled or taken directly from the DS1 spacecraft.[1] For example, systems that would grow with the size of the spacecraft (such as the structural mass or thermal protection system) are computed as a percentage of the spacecraft's dry mass (m_{dry}). In Table 1 the SEP tankage mass is computed as 15% of the xenon propellant mass (m_{prop}), and the solar array mass is the product of specific mass and input power at 1 AU from the sun (P_0, in kilowatts). Specific mass is fixed at 25 kg/kW and represents the DS1 array technology. The electric propulsion system consists of the same 30-cm ion thrusters and power-processing units (PPUs) as used in DS1. One PPU can process the power for two ion thrusters; therefore, additional PPUs must be added for spacecraft using more than two thrusters.

The spacecraft mass after injection into heliocentric space is

$$m_0 = m_{\text{system}} + m_{\text{prop}} + m_{\text{P/L}} \tag{1}$$

where m_{system} is the total spacecraft system mass (from Table 1) and $m_{\text{P/L}}$ is the payload mass. Injected mass m_0 is computed from Delta

Table 1 Spacecraft system mass breakdown

Spacecraft system	Mass contribution
Structure	0.21 m_{dry}
Thermal protection	0.03 m_{dry}
Electric propulsion	
Ion thruster	8.3 kg (each)
Power processing unit	15 kg (each)
Digital control unit	3 kg
Xenon tank and feed lines	0.15 m_{prop}
Engine gimbal	20 kg (each)
Power	
Solar array	(25 kg/kW)(P_0)
Cabling	0.04 m_{dry}
Batteries	45 kg
Attitude control	
Reaction jets	10 kg
Hydrazine propellant	30 kg
Electronics	12 kg
Attitude sensors	6 kg
Communication	15 kg

Received 26 April 2000; accepted for publication 29 June 2000.

*Associate Professor, Mechanical and Aerospace Engineering Department. Senior Member AIAA.

Table 2 Maximum payload transfers to comet Wilson-Harrington

Launch date, mo-day-yr	C_3, km^2/s^2	m_0, kg	$m_{P/L}$, kg	m_{prop}, kg	P_0, kW	Rendezvous date, days before T[a]	Trip time, yr
6-21-05	1.32	1253.2	385.6	224	3.77	0	4.34
7-24-05	1.93	1237.3	324.0	240	5.22	30	4.17
9-17-05	7.72	1097.0	183.5	240	6.80	60	3.93
10-17-05	13.69	970.3	53.2	240	8.36	90	3.80
6-20-05	12.99	984.3	311.3	160	2.96	0	4.34
8-20-05[b]	14.15	961.1	263.5[b]	160	4.20	30	4.09
9-12-05	19.94	854.2	156.4	160	5.41	60	3.95
9-4-05	24.88	772.8	62.1	160	6.84	90	3.89
4-27-05	37.13	603.9	156.4	80	2.12	0	4.49
5-11-05	38.88	583.0	126.2	80	2.72	30	4.37
5-11-05	46.11	503.8	52.1	80	3.41	60	4.29
5-8-05	52.57	442.1	−12.8	80	4.22	90	4.21

[a] T = perihelion date for Wilson-Harrington (23 Oct. 2009). [b] Baseline mission.

launch vehicle performance curves with launch energy C_3 as the independent variable.[9] Dry mass m_{dry} is the sum of system mass m_{system} (without the hydrazine propellant mass) and payload mass $m_{P/L}$. In the optimization process the design variables C_3 and P_0 will significantly affect the spacecraft's mass distribution and ultimately the payload mass.

It is assumed that the specific impulse I_{sp} for the ion thruster is fixed at 3360 s over the entire mission (no engine throttling) and that engine efficiency is a constant 66%. For this analysis the input power to the SEP system P is assumed to have an inverse-square relation with respect to radial distance from the sun (r):

$$P = P_0 / r^2 \tag{2}$$

Results

Several maximum-payload rendezvous trajectories to WH were computed using a variety of thrust-coast arc sequences and multiple-engine combinations. Initial trajectory solutions demonstrated large payload masses for rendezvous conditions well past the comet's perihelion passage. However, these solutions are not desirable to the scientific community because comets are most active near perihelion. Because the period of WH is 4.4 yr, rendezvous after perihelion would make scientific measurements near perihelion prohibitive because of the mission lifetime constraints. Therefore, an additional constraint for preperihelion rendezvous was imposed in order to maximize the mission's scientific return. This additional rendezvous constraint complicated the mission design and resulted in a significant continuous decrease in payload mass as the rendezvous date was pushed earlier from 23 October 2009 (perihelion for WH). The optimal payload for rendezvous at perihelion with three ion thrusters was found to be 213 kg and the trip time for this orbit transfer was 4.05 yr. Employing an Earth gravity assist (EGA) after a burn-coast sequence dramatically increased the payload mass for preperihelion rendezvous without significantly increasing the transfer time. Several maximum-payload transfers are presented in Table 2. All optimal transfers in Table 2 use a burn-coast-EGA-coast-burn flight program. Including additional burn and coast arcs did not increase payload. Table 2 presents optimal transfers for rendezvous at perihelion T and 30, 60, and 90 days before perihelion. Three sets of propellant constraints are imposed: $m_{prop} \leq 240$ kg, $m_{prop} \leq 160$ kg, and $m_{prop} \leq 80$ kg (three, two, and one ion thrusters). Table 2 shows that payload mass continually decreases as the rendezvous is moved ahead of perihelion. In addition, payload increases, and energy C_3 provided by the Delta 7925 decreases with the addition of ion thrusters (i.e., electric propulsion is more efficient than chemical propulsion). Launch energy becomes large for the one-thruster cases. Input power P_0 increases with the number of ion engines and steadily increases as rendezvous date is moved ahead of T. Table 2 provides a good survey of the mission design space and allows mission designers to select the best trade between payload mass, scientific return (rendezvous date), and mission complexity and cost (number of ion engines and P_0).

A nominal baseline mission for rendezvous with WH is selected from the optimal transfers presented in Table 2. The optimal transfer using two ion engines ($m_{prop} = 160$ kg) with a rendezvous 30 days before perihelion demonstrates a good trade between performance, scientific return, and mission complexity. A spacecraft with two ion thrusters only requires one PPU for power processing. The payload mass for this baseline case is large (263.5 kg), and input power is reasonable (4.2 kW). For earlier preperihelion rendezvous the new spacecraft mass characteristics can be interpolated from the solutions presented in Table 2. For example, a two-engine spacecraft can deliver a 200-kg payload 47 days before perihelion.

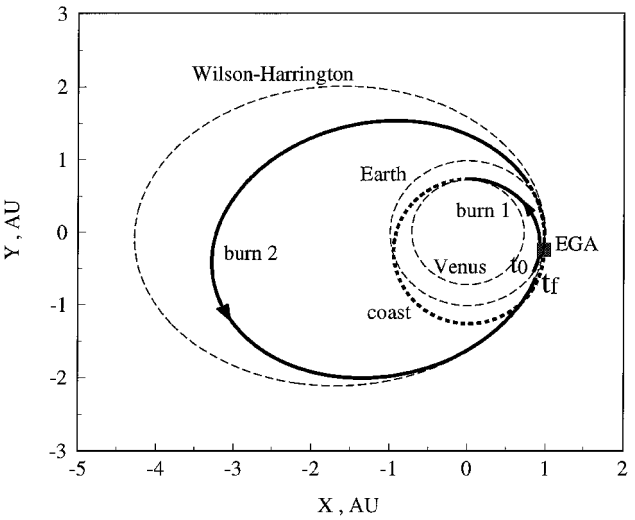

Fig. 1 Maximum-payload trajectory with two ion thrusters.

Figure 1 shows the baseline trajectory to WH for the two-engine spacecraft. The hyperbolic excess velocity vector provided by the Delta 7925 is nearly opposite the Earth's velocity vector, and therefore the spacecraft approaches the sun after injection into heliocentric space. The first SEP burn arc starts immediately after injection (20 August 2005) and lasts 94 days. The spacecraft begins a coast arc near the orbit of Venus that lasts 290 days until the EGA is performed on 8 September 2006. Earth flyby altitude is 350 km (minimum allowable altitude). The second SEP burn starts on 27 October 2006 (49 days after the EGA) and lasts 2.9 yr until rendezvous with WH on 24 September 2009. The total transfer time is 4.1 yr.

Conclusions

Several maximum-payload rendezvous trajectories to the short-period comet WH using SEP have been obtained. The mission design incorporates a detailed accounting of the spacecraft system mass as well as current-term electric propulsion technology. Constraints on the ion thruster lifetime and comet rendezvous date help assess design tradeoffs between payload mass, mission complexity, and scientific return. The results show that an SEP spacecraft with two ion thrusters can deliver a scientific payload mass of 263 kg 30 days before the comet's perihelion pass. These results suggest that a comet rendezvous mission utilizing SEP and a small launch vehicle is feasible and therefore may be a potential candidate for a Discovery-class mission.

Acknowledgments

The author would like to thank Robert W. Farquhar at the Johns Hopkins University, Applied Physics Laboratory and Donald K.

Yeomans at the Jet Propulsion Laboratory, California Institute of Technology, for their helpful insights during the course of this work.

References

[1]Rayman, M. D., and Lehman, D. H., "NASA's First New Millennium Deep-Space Technology Validation Flight," International Academy of Astronautics, IAA Paper L-0502, April 1996.

[2]Williams, S. N., and Coverstone-Carroll, V., "Mars Missions Using Solar Electric Propulsion," *Journal of Spacecraft and Rockets*, Vol. 37, No. 1, 2000, pp. 71–77.

[3]Kluever, C. A., and Abu-Saymeh, M., "Mercury Mission Design Using Solar Electric Propulsion Spacecraft," *Journal of Spacecraft and Rockets*, Vol. 35, No. 3, 1998, pp. 411–413.

[4]Sauer, C. G., "Solar Electric Performance for Medlite and Delta Class Planetary Missions," American Astronautical Society, AAS Paper 97-726, Aug. 1997.

[5]Sims, J. A., "Trajectories to Comets Using Solar Electric Propulsion," American Astronautical Society, AAS Paper 00-134, Jan. 2000.

[6]Kluever, C. A., "Optimal Interplanetary Trajectories by Direct Method Techniques," *Journal of the Astronautical Sciences*, Vol. 45, No. 3, 1997, pp. 247–262.

[7]Pouliot, M. R., "CONOPT2: A Rapidly Convergent Constrained Trajectory Optimization Program for TRAJEX," Convair Div., General Dynamics, GDC-SP-82-008, San Diego, CA, Jan. 1982.

[8]Williams, S. N., "An Introduction to the Use of VARITOP: a General Purpose Low-Thrust Trajectory Optimization Program," Jet Propulsion Lab., California Inst. of Technology, JPL D-11475, Pasadena, CA, Jan. 1994.

[9]"Delta II Payload Planners Guide," Boeing Co. Space and Communications Group, MDC H3224D, Huntington Beach, CA, April 1996.

D. B. Spencer
Associate Editor

Numerical Heat Transfer Study over Spiked Blunt Bodies at Mach 6.8

R. C. Mehta*
Vikram Sarabhai Space Center, Trivandrum 695 022, India

Introduction

HIGH-SPEED vehicles are designed to withstand severe aerodynamic heating conditions. Such vehicles include hypervelocity projectiles, reentry payload modules, and hypersonic aircraft. Maximum heating and the consequent potential for material erosion are typical problems associated in the nose region of the blunt body. For flight velocities of 2–4 km/s, the nose region experiences high heating rates, and material ablation may contribute to unacceptable perturbations in the vehicle's aerodynamic characteristics and flight path. As an example of the severity of the heating, the stagnation temperature at sea level for a velocity of about 3.1 km/s, that is, about Mach 8.9, corresponds to the melting point of tungsten. Therefore, there exists a need to develop an active or passive technique to reduce the heating rates in the vicinity of the nosetip region of the vehicle. Heat flux can be reduced by attaching a forward facing spike on the blunt nose of the vehicle. The spike is also an effective way to reduce the aerodynamic drag due to the reduced dynamic pressure in the separated flow region.[1]

Several experimental studies have been conducted to examine the forebody flowfield of the spiked blunt body. Most of the experimental investigations conducted in the 1950s concentrated on issues related to high pressures and heating rates around such configurations and possible mechanisms to reduce them. Stadler and Nielsen[2] carried out experiments on a hemisphere–cylinder configuration at freestream Mach numbers of 1.5, 2.67, and 5.0, and a Reynolds number in the range of 0.16×10^6–0.85×10^6 based on the diameter of the cylinder. Their experiments indicated a reduction in surface pressure and, consequently, the drag, with the attachment of the forward facing spike. However, an increase in heat transfer rates due to the spike were shown in comparison with the clean configuration. The increase in heat-transfer rates were attributed to the separated turbulent boundary layer periodically impinging on the outer region of the boundary layer on the blunt nose. The experimental investigation of Bogdonoff and Vas[3] indicated an initial drop in pressure at the nose of the forebody with increased spike length up to an L/D ratio of 3 (where L is the spike length and D is cylinder diameter). Chapman[4] found theoretically that the heat transfer across the separated laminar boundary layer was reduced to about 56% of the level associated with the attached laminar boundary layer. Crawford[5] experimentally investigated the effect of the spike length on the nature of the flowfield, the surface pressure distribution, and the heat flux variation for a freestream Mach number of 6.8 and Reynolds number 0.12×10^6–1.5×10^6 based on the cylinder diameter. According to his experimental analysis, the drag and the heat flux were reduced when the spike was lengthened, but the drag was not influenced by the spike length when the latter exceeds the blunt-body diameter by roughly four times.

These experimental investigations provide insight into the characteristics of the separated region created by an adverse pressure gradient and shock/boundary-layer interaction over the blunt nose. Unsteadiness of the flow caused by the spike of the blunt body was examined by Maull[6] in 1960. It was found that the shock wave around the body oscillates when the nose has a plane shape. Wood[7] investigated experimentally the flowfield over the spiked cone and found that the shape and size of a region of separated flow is controlled primarily by the flow near the reattachment point. Fluctuating pressures in spiked-induced flow separation was observed experimentally by Guenther and Reding.[8]

The features of the supersonic flowfield can be delineated through these experimental investigations. It is characterized by a conical shock wave from the tip of the spike, a reattachment shock wave on the blunt body, and a separated flow region ahead of the blunt body. A schematic of the flowfield over the spiked blunt body is shown in Fig. 1a. This flowfield has also been numerically investigated and physical aspects of the flowfield have been described. Yamauchi et al.[9] have numerically investigated the flowfield around a spiked blunt body at freestream Mach numbers of 2.01, 4.15, and 6.80 for different ratios of L/D. The focus of their analysis was to investigate the mechanism of drag reduction and the flowfield pattern at different freestream Mach numbers and spike lengths. However, flowfields around a spiked blunt body include phenomena that have not been described previously. In the present work, fluid dynamics and heat transfer studies were performed for a freestream Mach number of 6.8 for different spike lengths and for a Reynolds number of 0.14×10^6 based on the diameter of the hemispherical cap.

Governing Equations and Numerical Method

The time-dependent axisymmetric compressible Navier–Stokes equations were written in integral form, and the system of equations was augmented by the ideal gas law for solution. The coefficient of molecular viscosity was calculated according to Sutherland's law. The flow was assumed to be laminar, which is consistent with the experimental study of Crawford[5] and the numerical simulation of Yamauchi et al.[9]

The flowfield code employs a finite volume discretization technique. The spatial and temporal terms are decoupled using the method of lines. The spatial computational domain was divided into a finite number of nonoverlapping quadrilateral cells. Thus, the discretized solution to the governing equations results in a set of volume-averaged state variables of mass, momentum, and energy, which are in balance with their area-averaged fluxes (inviscid and viscous) across the cell faces.[10] The finite volume code constructed in this manner reduces to a central difference scheme and is second-order accurate in space provided that the mesh is smooth enough. The cell-centered spatial discretization scheme is nondissipative; therefore, artificial dissipation terms are included as a blend of a Laplacian and biharmonic operator in a manner analogous to the second and fourth difference. The artificial dissipation term was added explicitly to prevent numerical oscillations near shock waves to

Received 8 February 2000; accepted for publication 5 May 2000.

*Engineer, Aerodynamics Division. Senior Member AIAA.